Effect of electronic topological transitions on the calculations of some Zn and Fe properties

2005 J. Phys.: Condens. Matter 17 559

(http://iopscience.iop.org/0953-8984/17/3/014)

INSTITUTE OF PHYSICS PUBLISHING JOURNAL OF PHYSICS: CONDENSED MATTER

J. Phys.: Condens. Matter **17** (2005) 559–569 doi:10.1088/0953-8984/17/3/014

Effect of electronic topological transitions on the calculations of some Zn and Fe properties

G V Sin'ko and N A Smirnov

Russian Federal Nuclear Center—Institute of Technical Physics, Snezhinsk 456770, Russia

E-mail: gevas@uniterra.ru

Received 23 June 2004, in final form 12 December 2004
Published 7 January 2005
Online at stacks.iop.org/JPhysCM/17/559

Abstract

Based on the detailed *ab initio* calculations of electronic structure for hcp-zinc and bcc-ferromagnetic iron, we made an attempt to study a scale of anomalies emerging in the calculations of elastic properties of these crystals as functions of pressure, and determine a relation between these anomalies and electronic topological transitions. Our calculations give grounds to believe that an electronic topological transition in itself is not a cause of significant anomalies in elastic properties of crystals but is, probably, an indicator of rearrangement of the crystal energy spectrum: an indicator which is not even always present. In some cases such rearrangement can cause significant anomalies in elastic and other properties of the crystal.

As suggested by Lifshits [1] in 1960, electronic topological transitions (ETTs) in the energy spectrum of crystals may cause anomalies in their elastic and thermodynamic properties. However, the issue of the quantitative magnitude of those anomalies remains open because of the qualitative nature of paper [1] and later ones [2, 3] related to that topic. ETT-related anomalies of the crystal properties were observed in *ab initio* calculations as well, which in some cases gave grounds to explain anomalies experimentally detected in the crystal properties through the occurrence of ETTs. One of the best known attempts to explain the observed anomalies in the crystal properties through electronic topological transitions is associated with zinc. During the recent decade an active discussion has been focused on the problem of whether there exists a volume-dependent c/a ratio anomaly at $c/a = \sqrt{3}$ in the hcp structure of zinc and whether this anomaly is associated with an ETT. A detailed description of the discussion and relevant references are given in [4]. We will mention only some papers which aroused interest in the anomaly in zinc [5–8] and initiated similar work in cadmium [9].

It has been worked out by now that experiments indicating the existence of the anomaly were set up so that they did not provide hydrostatic compression (see [10]). Later experiments [10, 11] did not detect any anomaly near $c/a = \sqrt{3}$ exceeding an experimental error.

When the number of $\vec{k}$ points in integration over the Brillouin zone increased essentially, the previously computed anomaly in lattice parameters under compression disappeared [12], in agreement with the recent experiments. However, it should be noted that recently that result was called into question in [13].

This situation conveys the suggestion that similarly to experiments fictitious anomalies might occur in the calculations due to insufficient accuracy in the ETT-affected areas. Actual anomalies discussed by Lifshits [1] are probably rather small, at least in elastic properties of the crystals. The scale and location of fictitious anomalies are likely to depend on the calculation accuracy and this can be noticed when comparing the results obtained by different authors. This paper is an attempt to study in detail the effect the calculation accuracy produces on the lattice parameters at which ETTs emerge. Another issue we studied is how the calculation accuracy influences the scale of the fictitious anomaly emerging in the calculation of the volume dependence of the equilibrium c/a ratio in zinc. We also explored an effect of the calculation accuracy on the calculated elastic properties of zinc in the vicinity of the ETT. We used a number of $\vec{k}$ points in the Brillouin zone as an indicator of the calculation accuracy and a quantity

$$\frac{1}{V}\frac{\mathrm{d}^2E}{\mathrm{d}(c/a)^2}\bigg|_{\substack{c/a=c_0/a_0\\ V=\mathrm{const}}} = \frac{1}{2}(\tilde{C}_{11}+\tilde{C}_{12}) - 2\tilde{C}_{13} + \tilde{C}_{33},$$

as a characteristic of the elastic properties of zinc. Here $\tilde{C}_{ij}$ are elastic constants determining the mechanical stability of the crystal under pressure [14].

First we made detailed calculations of a number of characteristics of the hcp crystal of zinc under pressure using a larger number of $\vec{k}$-points in the Brillouin zone compared to other papers. The calculated results are given first. As expected, they reasonably agree with the data published so far. Then we tracked the variation of the ETT-related effects at a further increase of the then relatively high accuracy. We also give an example of bcc ferromagnetic iron (α-iron), where we believe an actual anomaly takes place and is accompanied by the almost simultaneous emergence of eight ETTs [19]. However, in this case both the anomaly and the ETTs are likely to be caused by significant rearrangement of the energy spectrum which is well described even at a relatively small number of $\vec{k}$-points.

To obtain the results, we used the full potential linear muffin-tin orbital method (FPLMTO) [15], which worked well in our previous studies [14, 16–19]. The exchange–correlation functional was selected in the form offered in [20] and [21] for zinc and iron, respectively. For each case we selected the form of exchange–correlation functional that would most accurately reproduce the crystal density under normal conditions. Both cases included gradient corrections [22]. 3s, 3p, 3d and 4s states in zinc and iron atoms are treated as valence electrons, and semi-core states were not treated separately. The basis set was formed of orbitals of s, p, d and f type. All relativistic effects were taken into account except spin–orbital coupling for valence electrons, which were treated in a scalar-relativistic approximation. The convergence criterion on the energy is set at 1×10^{-5} mRyd/cell.

In the prism-shaped Brillouin zone a mesh for integration over $\vec{k}$-space with the linear tetrahedron method was constructed by dividing each edge into the same number of parts. Most calculations were performed using a mesh with $40\times40\times40$ $\vec{k}$-points for zinc, and $50\times50\times50$ $\vec{k}$-points for α-iron. To estimate the dependence of the calculation results on the number of $\vec{k}$-points, this number was varied in a wide range. Figures below treat V_0 as the specific volume of the crystal at $P = 0$ and $T = 0$. Our calculations give $V_0 = 102.885$ (au)^3/atom for zinc, and $V_0 = 78.1576$ (au)^3/atom for α-iron. Extrapolation of the experimental data from [23] at $P = 0$ and $T = 0$ gives $V_0 = 100.5457$ (au)^3/atom for zinc and $V_0 = 79.0750$ (au)^3/atom for α-iron. The specific energy of hcp-zinc obtained in our calculations can be described with

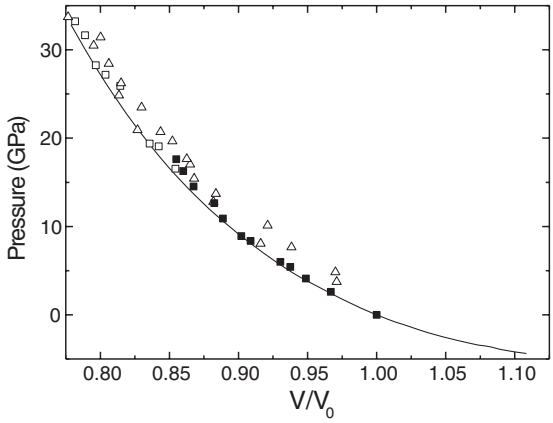

Figure 1. Pressure in hcp structure of zinc versus relative volume. Experimental data: solid squares— [11] at 40 K, open triangles— [25] at room temperature, open squares—data from the shock wave experiments recalculated to $T = 0$ K [26]. Our calculation is shown with a curve.

the formula of Rose *et al* [24] slightly modified by adding two additional parameters:

$$E_{0e}(V) = E_\infty - \Delta E(1 + y + \alpha y^2 + \beta y^3)\exp(-y), \tag{1}$$

where

$$y = \frac{1-x}{x}\frac{r_0}{\ell}, \qquad x = \left(\frac{v_0}{V}\right)^{1/3}, \qquad r_0 = \left(\frac{3v_0}{4\pi}\right)^{1/3}, \tag{2}$$

V is the specific volume, and v_0 is the specific volume at which $\mathrm{d}E_{0e}/\mathrm{d}V = 0$. Formula (1) is not as universal as the formula from [24], but it better approximates our results. Values v_0, ℓ, ΔE, E_∞, α and β in formula (1) are treated as parameters. The formula for pressure is derived from (1):

$$P_{0e}(V) = 3B_0 x(x-1)\left(1 + \frac{\alpha - 3\beta}{1-2\alpha}y + \frac{\beta}{1-2\alpha}y^2\right)\exp(-y), \tag{3}$$

where

$$B_0 = \frac{\Delta E(1-2\alpha)}{12\pi r_0 \ell^2}.$$

Selection of the parameters resulted in the following:

$$\begin{aligned} &v_0 = 0.140\,43\ \mathrm{cm^3\ g^{-1}}, \qquad \ell = 0.159\,25\ \mathrm{cm\ g^{-1}},\\ &\Delta E = E_\infty = 288.732\ \mathrm{kJ\ g^{-1}},\\ &\alpha = 0.467\,07, \qquad \beta = 0.223\,34. \end{aligned} \tag{4}$$

Approximation of the calculated specific energy of hcp-zinc made according to formula (1) with parameters (4) gives an error within the error of our computations.

It is worth noting that when using the results of *ab initio* calculations of cold curves in practice it is possible to somewhat improve agreement with the available experimental data by using formulae (1) and (3) to represent the cold energy and pressure of the actual system in the following form:

$$E_{\mathrm{col}}(V) = E_{0e}(v_0 \cdot \xi), \qquad P_{\mathrm{col}}(V) = \frac{v_0}{V_0}P_{0e}(v_0 \cdot \xi), \tag{5}$$

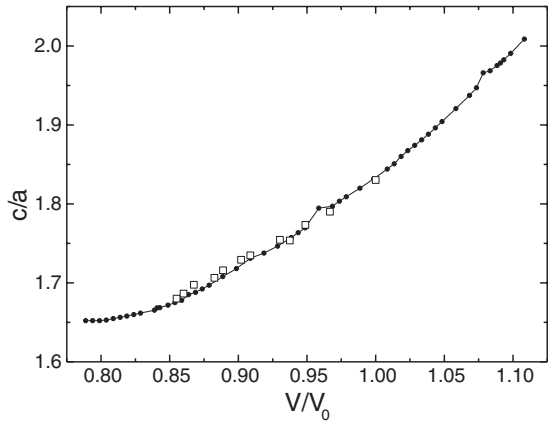

Figure 2. Equilibrium ratio c/a for hcp-structure zinc versus relative volume. The open squares stand for experiment [11], and the solid curve with dots corresponds to our calculation with a $40 \times 40 \times 40$ mesh.

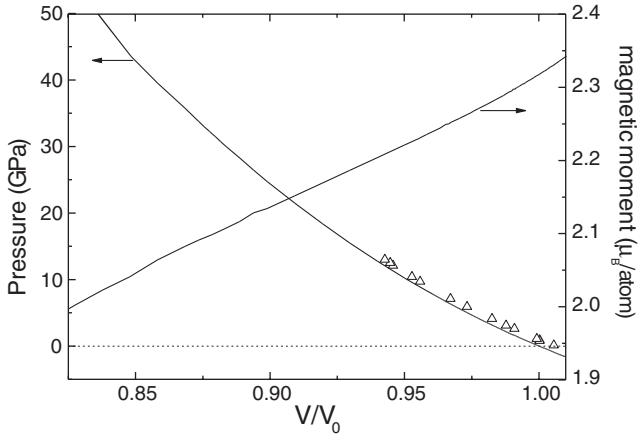

Figure 3. Pressure and specific magnetic moment for a compressed α-iron crystal versus relative volume. Solid curves stand for calculations and triangles correspond to experiment [30].

where $\xi = V/V_0$, V_0 is the experimental specific volume at $T = 0$ and $P = 0$. Figure 1 shows the calculated pressure in a zinc crystal versus the relative volume as compared with the experimental data from [11, 25, 26].

Figure 2 presents our calculations of the equilibrium ratio c/a in zinc versus the relative volume at $T = 0$ K and the available experimental data at $T = 40$ K [11]. The $c/a(V/V_0)$ points in figure 2 were found from the minima of $E(c/a)$ calculated at constant V.

The following results were obtained for iron. Specific volume, bulk modulus and its pressure derivative at $T = 0$ and $P = 0$ for α-iron from our calculations and calculations by other authors are given in table 1 as well as the experimental data under normal conditions. The calculated volume dependences of pressure and specific magnetic moment for compressed α-iron crystal are shown in figure 3. This figure also gives the results of the experiments determining the compressibility of α-iron. Rather good agreement between the calculations

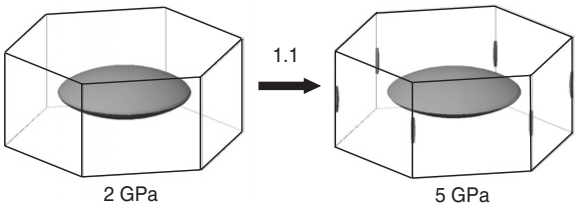

Figure 4. Change in the Fermi surface of zinc within the first partially occupied band.

Table 1. Calculated ($T = 0$ K) and experimental values of specific volume V_0, bulk modulus B_0, pressure derivative of bulk modulus B_0' and specific magnetic moment μ for crystals of α-iron under atmospheric pressure.

	V_0 ((au)^3/atom)	B_0 (GPa)	B_0'	μ (μ_B)
Calculations				
This work	78.158	168.6	5.7	2.31
Leung *et al* [27]	80.629	174.0	—	2.20
Dufek *et al* [28]	76.780	215.0	—	2.21
Stixrude *et al* [29]	76.840	189.0	4.9	2.17
Experiments (room temperature)				
Pearson [31]	79.063	—	—	2.12
Gschneidner [32]	79.496	171.6	—	—
Kittel [33]	79.845	168.3	—	2.22
Jephcoat *et al* [34]	79.510	172.0	—	—
Guinan *et al* [35]	—	166.4	5.29	—
Vaidya *et al* [36]	—	175.8	7.67	—

and available experimental data proves the high accuracy of the calculations both for zinc and for iron crystals.

Our calculations have shown that under ambient conditions the Fermi surface of zinc consists of three parts corresponding to three partially occupied energy bands, which we will number from the upper one downwards. Seven ETTs are detected within the pressure range from -5 to 35 GPa. One ETT occurs in the first band, four in the second band and two in the third one. Figures 4–6 illustrate the correspondent topological changes in the Fermi surface. Pressures corresponding to the Fermi surfaces shown in figures 4–6 were obtained in the calculations with $40 \times 40 \times 40$ mesh. But keep in mind that pressures at which ETTs occur significantly depend on the calculation accuracy. Figure 7 shows the band-structure dispersion $E(\vec{k})$ at $P = 0$ and also prior to and after the ETTs marked as 2.4 in figure 5 and 3.2 in figure 6.

The curve showing specific energy versus strain at constant volume in the vicinity of the ETT is parabola-like with ETT-induced wavy perturbation. The amplitude of this perturbation depends on the calculation accuracy. As V/V_0 varies in the vicinity of the ETT the associated perturbation moves from one parabola branch to another, and as it passes the parabola minimum it changes dramatically the volume dependence of the ratio c/a. This manifests itself as an anomaly in the calculated volume dependence of the ratio c/a. Figure 8 shows the specific energy versus ratio c/a at $V/V_0 = 0.96$ at the moment when the ETT-induced perturbation passes the parabola minimum in the calculation on the $40 \times 40 \times 40$ mesh. Figure 8 gives the density of the states on the Fermi surface versus the ratio c/a at $V/V_0 = 0.96$ as well. The density of states on the Fermi surface as a function of c/a has peaks corresponding to the

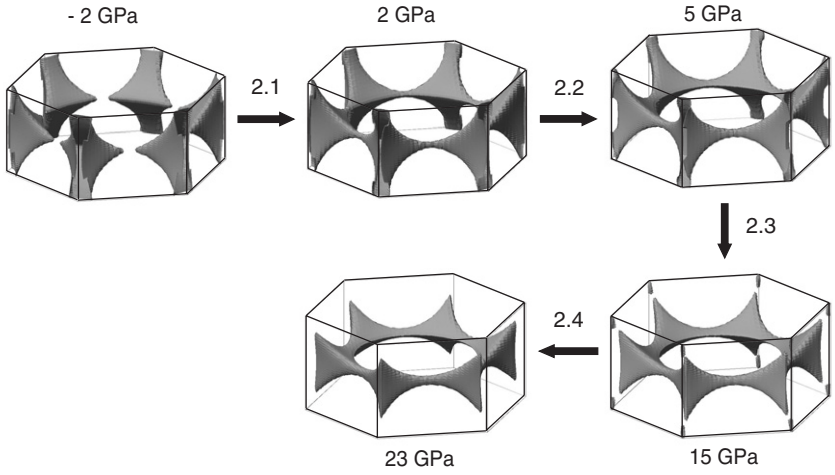

Figure 5. Change in the Fermi surface of zinc within the second partially occupied band.

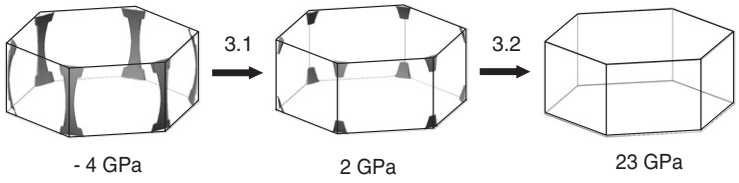

Figure 6. Change in the Fermi surface of zinc within the third partially occupied band.

topological changes of the Fermi surface labelled as 1.1 and 2.2 in figures 4 and 5, respectively. This value as a function of V/V_0 has peaks too. The shape of the $E(c/a)$ curve in figure 8 shows that the calculated dependence of the equilibrium parameter c/a on specific volume can have minor anomalies like isostructural transitions at those values of specific volume at which the ETT occurs near equilibrium c/a. These anomalies are noticeable in figure 2. Locations of anomalies, which are noticeable in figure 2, were determined in the calculations on the $(40 \times 40 \times 40)$ mesh. However, when the number of k-points changes, the location of anomalies shifts together with the location of ETTs. Figure 8 also shows that the elastic constants are very sensitive to the accuracy of ETT description. This corresponds to the case when the accuracy of the elastic constant calculation is completely determined by the ETT description accuracy. If, for example, the dependence in figure 8 is approximated with a parabola, the second derivative can vary more than by an order of magnitude depending on the interval within which the approximation is made.

These conclusions can be drawn from the calculations on a rather fine $40 \times 40 \times 40$ mesh within the Brillouin zone.

Our later calculations have shown that an answer to the question of at what pressure this or that ETT occurs, and what size the effects associated with it have, depends significantly on the number of k-point in the mesh used for integration over $\vec{k}$-space.

Figure 9 shows the density of states on the Fermi surface of zinc versus the ratio c/a for specific volume $V/V_0 = 0.96$ at different numbers of mesh points within the Brillouin zone. Peaks on the curves correspond to the ETTs labelled as 1.1 and 2.2 in figures 4 and 5,

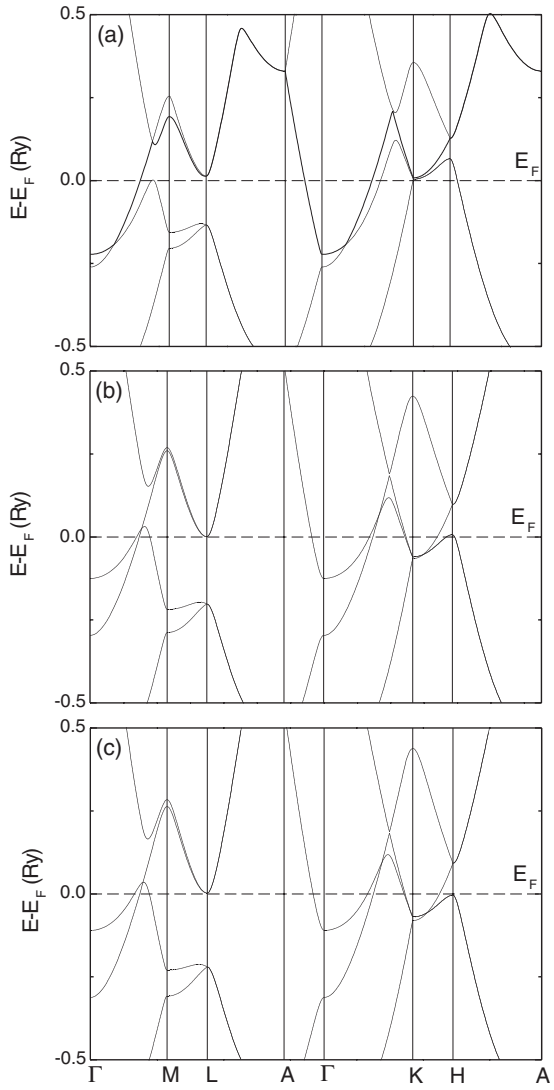

Figure 7. Hcp-zinc: band structure along high-symmetry directions in the first Brillouin zone around the Fermi energy. The upper, middle and lower panels show the band structure at $P = 0$, 15 and 23 GPa, respectively.

respectively. If a dependence $E(c/a)$ similar to that in figure 8 is built for each curve in figure 9, the ETT-induced perturbation will appear to be located in different parabola areas. Correspondingly, approximation of each curve will give an individual equilibrium ratio c/a and an individual value of the second derivative at the minimum, that means that individual elastic constants will correspond to the appropriate calculation accuracy. From figure 9 it is obvious that even an $80 \times 80 \times 80$ mesh containing 512 000 points in the Brillouin zone is insufficient for determining ETT positions for zinc. The number of $\vec{k}$-points in the meshes used seems insufficient even for making convergence to the exact result smooth.

In addition, an obvious trend is observed which shows that the ETT-induced perturbations in the density of states on the Fermi surface (and, therefore, in energy and in elastic constants)

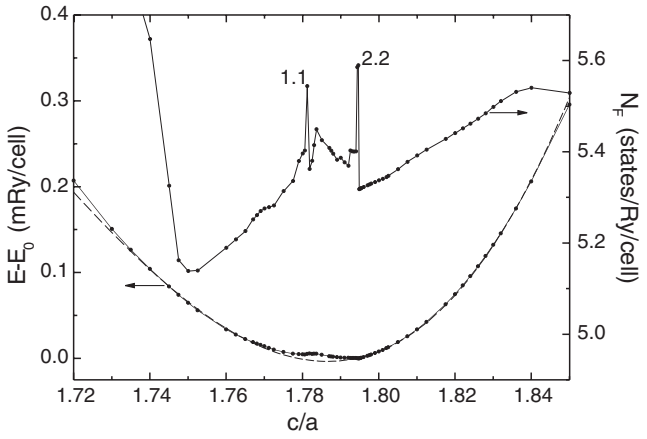

Figure 8. Hcp-zinc: calculated specific energy and density of states on the Fermi surface versus ratio c/a at $V/V_0 = 0.96$ and the $(40 \times 40 \times 40)$ mesh. The dashed curve gives an approximation of $E(c/a)$ with a cubic polynomial.

decrease with the increase of mesh point number in $\vec{k}$-space. It is possible to suppose that a significant effect of the isolated ETT on the elastic properties of crystals previously observed in the calculations done by different authors results from the use of insufficiently fine meshes. At the same time, in the cases when crystal strain is not accompanied by topological changes of the Fermi surface and dramatic changes in the density of states on the Fermi surface, the elastic constants can be calculated at a rather good accuracy even on the coarse meshes.

Our calculations give grounds to believe that an ETT in itself is not a cause of significant anomalies in elastic properties of crystals but is, probably, an indicator of rearrangement of the crystal energy spectrum: an indicator which is not even always present. In some cases such rearrangement can cause significant anomalies in the elastic and other properties of the crystal.

A crystal of α-iron is an interesting example. Calculations show [19] that α-iron experiences 12 ETTs within the range of $0.85 \leqslant V/V_0 \leqslant 1.2$. Eight of them happen when specific volume varies within 1%, and this evidences a significant rearrangement of energy spectrum, which turns out to cause loss of mechanical stability of the crystal. Topological changes taking place on the Fermi surface within the compression range of $0.85 \leqslant V/V_0 \leqslant 1.2$ are illustrated in [19]. The density of states on the Fermi surface as a function of relative volume which reflects this spectrum rearrangement is shown in figure 10. In this case variation of the number of mesh points for integration over $\vec{k}$-space did not cause any significant change in the results. Spectrum rearrangement results in a significant change in the number of electrons with positive and negative spin projection, thus causing a sudden change in the magnetic moment of the crystal. In addition, an area appears in the dependence of pressure on the relative volume, where $\mathrm{d}P/\mathrm{d}V > 0$, and this means that the α-iron crystal has lost its mechanical stability. Figure 11 shows the dependence of the pressure and magnetic moment in an α-iron crystal on the relative volume in the anomaly area.

As far as we know anomalies in the volume dependences of crystal specific energy and pressure similar to those shown in figure 11 have not been observed and reported yet in any theoretical or experimental works. So far only loss of mechanical stability by α-iron crystals at very high pressures has been reported [37]. Therefore, it would be extremely interesting to experimentally investigate α-iron crystals at negative pressures and low temperatures to detect

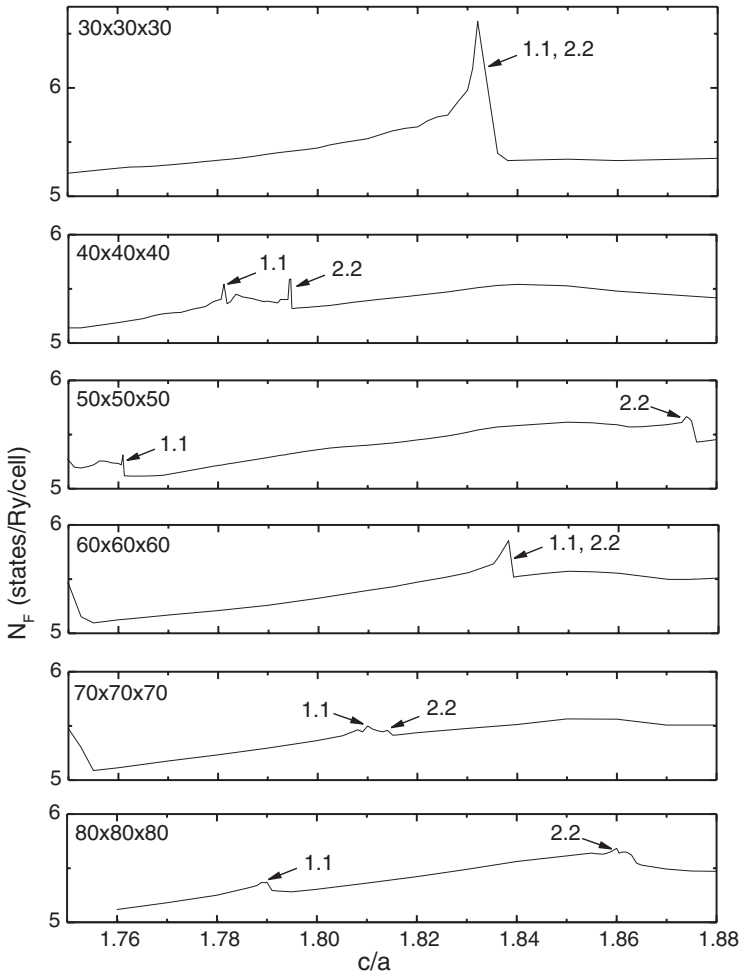

Figure 9. Density of states on the Fermi surface of hcp-zinc versus ratio c/a at $V/V_0 = 0.96$ calculated using different meshes within the Brillouin zone.

unusual elastic properties of these crystals. In this connection the new method of measuring the speed of sound proposed in [38] might be very helpful. It measures the speed of sound both in the compression area and at crystal tension. Experiments with the filiform α-iron crystals (whiskers) can also be useful. An abrupt change of magnetic moment of the iron sample at the moment when the shock wave reaches its surface can become indirect evidence of the existing anomaly in the elastic properties of α-iron.

Two important conclusions can be drawn from the obtained results. First, noticeable anomalies in the elastic properties of the crystal can take place within the density area where ETTs occur. However, the anomalies are probably caused not by ETTs themselves but by rather intensive rearrangement of the energy spectrum of the crystal during which the ETTs occur (or do not occur).

Second, the pressure at which this or that ETT occurs in zinc according to the calculations can significantly depend on the parameters determining the calculation accuracy, in particular, on the number of $\vec{k}$-points in the used mesh. For different meshes, the location of one and the

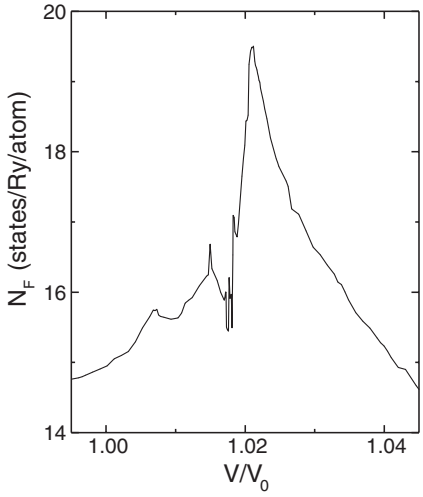

Figure 10. Density of states on the Fermi surface of α-iron as a function of relative volume.

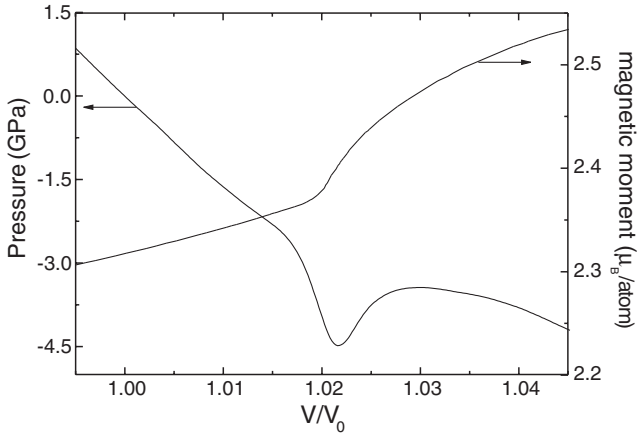

Figure 11. Pressure and magnetic moment of α-iron in the anomaly area versus relative volume.

same ETT and effects related to it can considerably differ even in the cases when calculations of specific energy beyond the ETT-affected area give very close results on those meshes. Thus, prior to determining the ETT location or its effect on the crystal properties from the calculated results, it is necessary to thoroughly investigate the dependence of the results on the number of $\vec{k}$-points in the used mesh and on other parameters influencing the accuracy of the numerical simulation. We have drawn this conclusion on the basis of calculations for zinc. It would be very interesting to check how general this conclusion is by studying other crystals.

Acknowledgments

This work was supported by the Russian Foundation for Basic Research (grant 04-02-17292) and the International Science and Technology Centre (project 1181).

References

[1] Lifshits I M 1960 *Zh. Eksp. Theor. Fiz.* **38** 1569
Lifshits I M 1960 *Sov. Phys.—JETP* **11** 1130 (Engl. Transl.)
[2] Naumov I I, Panin V E and Zhorovkov M F 1980 *Fiz. Met. Metalloved.* **50** 489
[3] Vaks V G and Trefilov A V 1988 *J. Phys. F: Met. Phys.* **18** 213
[4] Modak P, Rao R S and Godwal B K 2002 *J. Phys.: Condens. Matter* **14** 10927
[5] Meenakshi S, Vijayakumar V, Godwal B K and Sikka S K 1992 *Phys. Rev.* B **46** 14359
[6] Potzel W, Steiner M, Karzel H, Schiessl W, Kofferlein M, Kalvius G M and Blaha P 1995 *Phys. Rev. Lett.* **74** 1139
[7] Novikov D L, Freeman A J, Christensen N E, Svane A and Rodriguez C O 1997 *Phys. Rev.* B **56** 7206
[8] Olijnyk H, Jephcoat A P, Novikov D L and Christensen N E 2000 *Phys. Rev.* B **62** 5508
[9] Godwal B K, Meenakshi S and Rao R S 1997 *Phys. Rev.* B **56** 14871
[10] Takemura K 1999 *Phys. Rev.* B **60** 6171
[11] Takemura K 2002 *Phys. Rev.* B **65** 132107
[12] Steinle-Neumann G, Stixrude L and Cohen R E 2001 *Phys. Rev.* B **63** 054103
[13] Qiu S I and Marcus P M 2003 *J. Phys.: Condens. Matter* **15** L755
[14] Sin'ko G V and Smirnov N A 2002 *J. Phys.: Condens. Matter* **14** 6989
[15] Savrasov S Yu and Savrasov D Yu 1992 *Phys. Rev.* B **46** 12181
[16] Katsnelson M I, Sin'ko G V, Smirnov N A, Trefilov A V and Khromov K Yu 2000 *Phys. Rev.* B **61** 14420
[17] Sin'ko G V and Smirnov N A 2002 *JETP Lett.* **75** 217
[18] Sin'ko G V and Smirnov N A 2003 *5th Int. Symp. on High Dynamic Pressures (Saint-Malo, France)* vol 2, pp 301–12
[19] Sin'ko G V and Smirnov N A 2004 *JETP Lett.* **79** 665
[20] Gunnarson O and Lundqvist B I 1976 *Phys. Rev.* B **13** 4274
[21] Janak J F, Moruzzi V L and Williams A R 1975 *Phys. Rev.* B **12** 1257
[22] Perdew J P, Chevary J A, Vosko S H, Jackson K A, Pederson M R, Singh D J and Fiolhais C 1992 *Phys. Rev.* B **46** 6671
[23] Novikova S I 1974 *Thermal Expansion of Solids* (Moscow: Nauka)
[24] Rose J H, Smith J R, Guinea F and Ferrante J 1984 *Phys. Rev.* B **29** 2963
[25] Schulte O and Holzapfel W B 1996 *Phys. Rev.* B **53** 569
[26] Marsh S P 1980 *LASL Shock Hugoniot Data* (Berkeley, CA: University of California Press)
[27] Leung T C, Chan C T and Harmon B N 1991 *Phys. Rev.* B **44** 2923
[28] Dufek P, Blaha P and Schwarz K 1994 *Phys. Rev.* B **50** 7279
[29] Stixrude L, Cohen R E and Singh D J 1994 *Phys. Rev.* B **50** 6442
[30] Landolt–Bornstein 1988 *Structure Data of Elements and Intermetallic Phases* vol 14/III (Berlin: Springer)
[31] Pearson W B 1958 *Handbook of Lattice Spacings and Structures of Metals and Alloys* (New York: Pergamon)
[32] Gschneidner K A Jr 1964 *Solid State Phys.* **16** 275
[33] Kittel C 1996 *Introduction to Solid State Physics* (New York: Wiley)
[34] Jephcoat A P, Mao H K and Bell P M 1986 *J. Geophys. Res.* **91** 4677
[35] Guinan M W and Beshers D N 1968 *J. Phys. Chem. Solids* **29** 541
[36] Vaidya S N and Kennedy G C 1970 *J. Phys. Chem. Solids* **31** 2329
[37] Hong Ma, Qiu S L and Marcus P M 2002 *Phys. Rev.* B **66** 024113
[38] Bezruchko G S, Kanel G I and Razorenov S V 2004 *High Temp.* **42** 262
Bezruchko G S, Kanel G I and Razorenov S V 2004 *TVT* **42** 262 (in Russian)